

# Miniaturised triple-band antenna loaded with complementary concentric closed ring resonators with asymmetric coplanar waveguide-fed based on epsilon negative transmission line

ISSN 1751-8725  
 Received on 28th August 2017  
 Revised 14th April 2018  
 Accepted on 25th June 2018  
 E-First on 3rd September 2018  
 doi: 10.1049/iet-map.2018.5164  
 www.ietdl.org

Rajkishor Kumar<sup>1</sup>, Reshma Singh<sup>1</sup>, Raghvendra Kumar Chaudhary<sup>1</sup> ✉

<sup>1</sup>Department of Electronics Engineering, Indian Institute of Technology (Indian School of Mines), Dhanbad 826 004, India

✉ E-mail: raghvendra.chaudhary@gmail.com

**Abstract:** This study presents an open-ended triple-band miniaturised metamaterial (MTM) inspired antenna based on the epsilon negative-transmission line (ENG-TL). The zeroth-order resonance (ZOR) and first-order resonance (FOR) characteristics are implemented using the ENG-TL theory. The proposed MTM antenna consists of rectangular and square-shaped complementary concentric closed ring resonator (CCCR) in the left and right half of the asymmetric coplanar waveguide (CPW) ground plane, respectively. The CCCRR generates an extra coupling capacitance and inductance, which help for improving the gain at ZOR mode and better impedance matching at higher-order mode. The resonance characteristic of the antenna is controlled by the shunt elements due to its open-ended boundary condition. The proposed triple-band MTM antenna offers measured  $-10$  dB impedance bandwidths of 8.54% (1.12–1.22 GHz), 10.25% (2.22–2.46 GHz) and 35.75% (2.94–4.22 GHz). All these three bands show good impedance matching with appropriate gain and high radiation efficiency and also having an omnidirectional pattern in the  $xz$ -plane and dipolar type pattern in the  $yz$ -plane. The designed antenna shows an overall dimension of  $0.11\lambda_0 \times 0.11\lambda_0 \times 0.006\lambda_0$  at ZOR frequency (1.16 GHz).

## 1 Introduction

With the recent developments in modern wireless communication systems, miniaturised antennas with good impedance bandwidth and better far-field properties have more demand. The metamaterial (MTM) inspired antennas have excellent electromagnetic properties such as negative refractive index, anti-parallel group, and phase velocities and zero propagation constant [1–3] as compared with conventional antennas. Therefore, it has been widely used for designing compact antennas for wideband and multi-band applications [4–6]. The bandwidth enhancement technique of MTM antennas using split ring resonators is described in [7, 8]. The zeroth-order resonance (ZOR) is an excellent characteristic to miniaturise the antenna size because it is independent of the physical dimensions of the antenna and dependent on the distributed lumped parameters [9]. From the literature, mainly two methods have been reported to achieve ZOR. First by using composite right/left-handed transmission line and second by using an epsilon negative-transmission line (ENG-TL) [10, 11]. The formation of ZOR frequency depends on open-ended or short-ended boundary conditions. Therefore, it can be configured by using shunt inductor–capacitor (LC) parameters for open-ended and series-LC parameters for the short-ended case [12, 13]. Asymmetric coplanar waveguide (ACPW) is utilised to implement the antenna elements because it offers more design freedom compared with traditional CPW and also helps to enhance the antenna bandwidth [14]. The concepts of compact multi-band antennas are useful in the recent wireless communication systems such as Bluetooth, global positioning system, wireless local area network, wireless fidelity, worldwide interoperability for microwave access etc. to overcome the interference between other frequency bands and also individually tune the near and far-field properties [15–17].

In this paper, a compact open-ended triple-band MTM antenna based on the ENG-TL has been designed and developed for various wireless applications. By using the circuit parameters of ENG-TL, ZOR and first-order resonance (FOR) characteristics have been

analysed and verified. In case of open-ended condition, the ZOR and FOR characteristics have been tested by using shunt LC elements, i.e.  $L_L$  and  $C_R$  of the designed MTM antenna. The measured results of triple-band MTM antenna offers 8.54% (centred at 1.17 GHz), 10.25% (centred at 2.34 GHz) and 35.75% (centred at 3.58 GHz). In addition, the designed antenna offers better gain, better bandwidth and good radiation efficiency in all the three working bands and it is suitable for working in L-, S- and C-frequency bands.

## 2 Antenna theory and design

### 2.1 ENG-TL theory

Equivalent circuit diagram of the proposed ENG-TL is presented in Fig. 1. The left-handed equivalent shunt inductor  $L_L$  is formed by the current flow through the inductive thin strip having different lengths ( $L_{L1}$ ,  $L_{L2}$ ,  $L_{L3}$ ,  $L_{L4}$  and  $L_{L5}$ ), which is connected to the asymmetric ground plane and a stub [works as virtual ground ( $C_S$ )]. The right-handed equivalent series inductance  $L_R$  is resulted by the current flow through the main feed line and pentagonal-ring patch ( $L_{PT}$  and  $C_{PT}$ ). The shunt capacitances  $C_{R1}$  and  $C_{R2}$  are formed by the gap between the feed line and asymmetric ground planes. In addition,  $C_{11}$ ,  $C_{12}$ ,  $C_{13}$  and  $C_{21}$ ,  $C_{22}$ ,  $C_{23}$  are the coupling capacitance arising due to the gap between both sides of complementary concentric closed ring resonators (CCCRs). While  $L_{11}$ ,  $L_{12}$ ,  $L_{13}$ ,  $L_{14}$  and  $L_{21}$ ,  $L_{22}$ ,  $L_{23}$ ,  $L_{24}$  are the inductances generated on both sides of the asymmetric ground plane due to CCCRRs.

By using Bloch and Floquet theorem to the unit cell of periodic structures, the dispersion relation can be obtained and it is reported in [11, 18]

$$\beta_{\text{ENG-TL}}(\omega) = \frac{1}{p} \cos^{-1} \left[ 1 + \frac{Z_{\text{ENG}}(\omega) \times Y_{\text{ENG}}(\omega)}{2} \right] \quad (1)$$

where

$$Z_{ENG}(\omega) = j\omega L_R + \frac{j\omega L}{1 - \omega^2 LC} \quad (2)$$

$$Y_{ENG}(\omega) = (Y_1 + Y_2 + Y_3) \quad (3)$$

Here

$$Y_1 = j \left[ \omega C_{R1} + \frac{\omega C_{11}}{1 - \omega^2 C_{11} L_{11}} + \frac{\omega C_{12}}{1 - \omega^2 C_{12} L_{12}} + \frac{\omega C_{13}}{1 - \omega^2 C_{13} L_{13}} - \frac{1}{\omega L_{14}} \right] \quad (4)$$

$$Y_2 = \frac{1}{j\omega L_{L5}} + \frac{1}{j[\omega L_{L1} + \omega L_{L2} + \omega L_{L3} + \omega L_{L4} - (1/\omega C_S)]} \quad (5)$$

$$Y_3 = j \left[ \omega C_{R2} + \frac{\omega C_{21}}{1 - \omega^2 C_{21} L_{21}} + \frac{\omega C_{22}}{1 - \omega^2 C_{22} L_{22}} + \frac{\omega C_{23}}{1 - \omega^2 C_{23} L_{23}} - \frac{1}{\omega L_{24}} \right] \quad (6)$$

The propagation constant for the Bloch wave is denoted by  $\beta$  and  $p$  representing the length of the proposed unit cell. The resonance of the proposed ENG-TL-based triple-band MTM antenna is obtained when

$$\beta_n p = \frac{n\pi p}{l} = \frac{n\pi}{N} (n = 0, 1, 2, 3, 4, \dots, (N-1)) \quad (7)$$

where  $N$ ,  $l$  ( $= Np$ ) and  $n$  are the number of unit cells, total physical length and resonance modes of the resonator, respectively.

The proposed MTM antenna follows an open-ended boundary condition, so the input impedance ( $Z_{in}$ ) is seen from one end of resonator toward the other end. The load impedance is infinite ( $Z_L = \infty$ ). Therefore, the input impedance  $Z_{in}$  is given by [11]

$$Z_{in}^{Open} = -jZ_0 \cot(\beta l) \sim jZ_0 \frac{1}{\beta l} = -j\sqrt{\frac{Z'_{ENG}}{Y'_{ENG}}} \left( \frac{1}{-j\sqrt{Z'_{ENG} Y'_{ENG}}} \right) \frac{1}{l} = \frac{1}{Y'_{ENG}} \times \frac{1}{l} = \frac{1}{NpY} \quad (8)$$

From (7), when  $n=0$ , the propagation constant  $\beta=0$  and it represents ZOR mode and the resonant frequency of the ZOR mode is given by

$$\omega_{sh} = \omega_{ZOR} = \frac{1}{\sqrt{L'_L C'_R}} \quad (9)$$

where  $L'_L$  is the equivalent shunt inductance, which is a combination of different thin strip lengths.  $C'_R$  is the equivalent shunt capacitance which is formed by the combination of the gap of the feed line and the ground plane and the gap between CCCRRs.

From (9), it is clear that the ZOR frequency can be controlled by using shunt inductance ( $L'_L$ ) and capacitance ( $C'_R$ ) of the proposed MTM antenna.

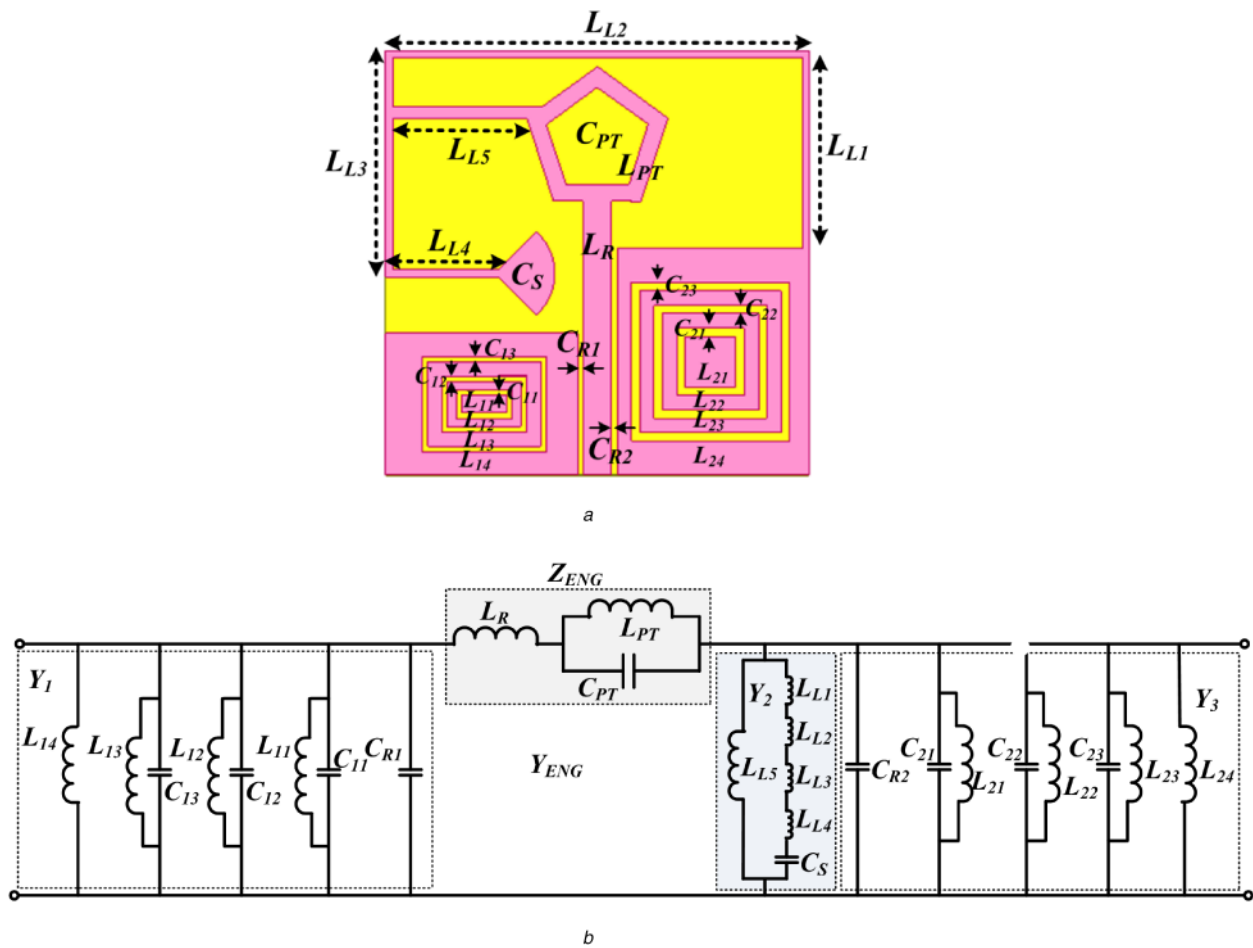


**Fig. 1** Proposed geometry and equivalent circuit diagram of a proposed antenna

(a) Proposed triple-band ENG-TL MTM antenna structure,

(b) Equivalent circuit diagram of the proposed antenna [ $L_R = 1.27$ ,  $L_{PT} = 19.33$ ,  $L_{L1} = 8.09$ ,  $L_{L2} = 4.66$ ,  $L_{L3} = 6.62$ ,  $L_{L4} = 11.13$ ,  $L_{L5} = 1.08$ ,  $L_{L11} = 5.47$ ,  $L_{L12} = 6.73$ ,  $L_{L13} = 13.56$ ,  $L_{L14} = 8.69$ ,  $L_{L21} = 13.37$ ,  $L_{L22} = 10.83$ ,  $L_{L23} = 4.42$ ,  $L_{L24} = 8.98$  all dimensions are in nH and  $C_{PT} = 4.95$ ,  $C_S = 2.10$ ,  $C_{R1} = 1.95$ ,  $C_{11} = 0.69$ ,  $C_{12} = 6.26$ ,  $C_{13} = 2.59$ ,  $C_{R2} = 0.783$ ,  $C_{21} = 3.13$ ,  $C_{22} = 2.84$ ,  $C_{23} = 2.05$  all dimensions are in pF

The FOR based on the ENG-TL occurs when  $n = 1$  [see from (7)] and the resonance frequency of FOR is given by [19]

$$\omega_{\text{FOR}} = \sqrt{\frac{1}{C'_R} \left( \frac{1}{L'_R} + \frac{1}{L'_L} \right)} \quad (10)$$

where  $L'_R$  is the equivalent series inductance, due to the feed line and hollow pentagonal.

It is clearly observed from (10) that the FOR depends on series as well as shunt parameters of the ENG-TL.

### 2.2 Antenna configuration

Fig. 2 depicts the configuration of the proposed triple-band MTM antenna having optimised dimensions in the caption. The proposed MTM antenna mainly consists of a signal line with hollow pentagonal-ring radiator, ACPW and CCCRR's on both sides of the asymmetric ground plane. The entire structure has been fabricated on low-cost Flame Retardant 4 (FR4) glass epoxy substrate having a thickness of 1.6 mm with a dielectric constant ( $\epsilon_r$ ) of 4.4, and loss tangent ( $\tan \delta$ ) of 0.025. The overall size of the proposed triple-band MTM antenna is  $0.11\lambda_0 \times 0.11\lambda_0 \times 0.006\lambda_0$  ( $30 \times 30 \times 1.6$  mm<sup>3</sup>), where  $\lambda_0$  is the free-space wavelength at ZOR frequency (1.16 GHz).

The proposed structure comprises of a pentagonal-ring patch which is connected to ground with thin stripline, the CCCRR's which are loaded on the asymmetric ground and a stub which is connected to the patch through thin stripline. The proposed antenna has been designed, such that ENG-TL structure can be realised. Some portion of the ground plane is eliminated, i.e. the asymmetrical ground plane has been utilised to decrease the electrical size of the antenna. Here, the radial stub is used as a virtual ground plane and it offers high capacitance.

### 2.3 Validation of ZOR and FOR modes

The concept of originating ZOR is well known and already established in the theory of CRLH-based structure. For validation of ZOR mode, parametric analysis has been carried out by varying width ( $W_{F3}$ ) of the thin stripline. Here, shunt inductance has been chosen for verifying the ZOR mode of the proposed MTM antenna. It can be seen from Fig. 3a that by increasing the width of stripline, the ZOR frequency is also increased. Since thin stripline represents the shunt inductance, its value can be changed by varying  $W_{F3}$ . From this analysis, it is confirmed that the ZOR frequency primarily depends on the shunt inductance, and follow the open-ended conditions [20]. It can be clearly observed in Fig. 3a that the FOR mode also exists in this proposed antenna because it depends on shunt as well as series parameters [19]. As per the literature survey, to validate the ZOR and FOR modes in the antenna structure; usually vector electric fields were plotted and  $E$ -fields are observed normal to the antenna structure. In this context, Fig. 3b depicts the  $E$ -field distribution at the ZOR frequency for cross-verifying the ZOR mode in the designed antenna. It can be observed that at a specified frequency (1.28 GHz), all field lines are in the same phase which confirms the validation of ZOR mode.

To verify the FOR mode of the proposed MTM antenna, the width of series inductance ( $L_R$ ) has been chosen. As the width of series inductance ( $W_F$ ) increases, the right-handed inductance ( $L_R$ ) decreases, which shifts the FOR to higher frequencies but ZOR remains constant as shown in Fig. 4a. Therefore, it can be concluded that the series, as well as shunt parameters, are responsible for shifting the FOR frequency in case of ENG-TL and it is verified by given (7). Fig. 4a confirms that in an open-ended case, the shift in ZOR frequency only depends on shunt parameters of the proposed antenna structure which is verified in (6). Fig. 4b depicts the  $E$ -field distribution at the FOR frequency (2.30 GHz) of the proposed antenna for cross-verifying the above claim. It can be observed from Fig. 4b that the hollow pentagonal patch and thin stripline are mainly responsible for the generation of FOR mode.

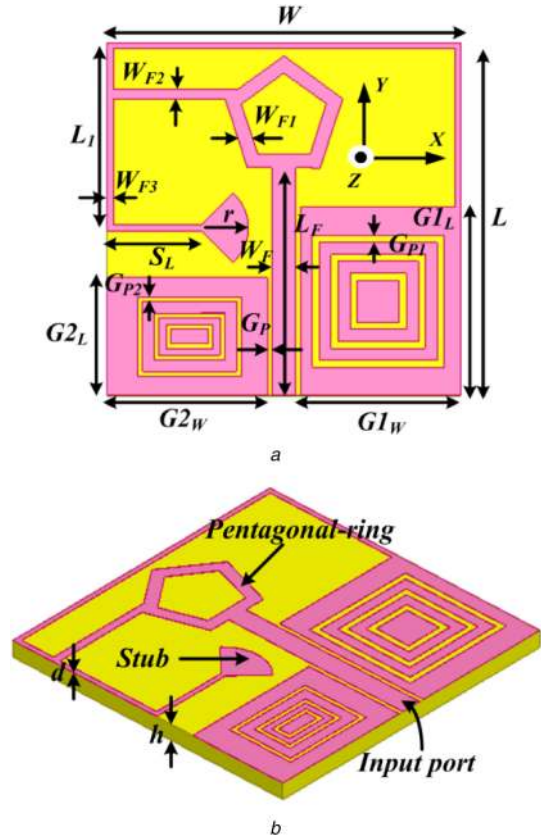


**Fig. 2** Geometry of the proposed triple-band MTM antenna

(a) Top view,

(b) Side view [ $L = 30$ ,  $W = 30$ ,  $h = 1.6$ ,  $L_f = 16$ ,  $L_1 = 15$ ,  $G_{1L} = 15$ ,  $G_1 W = 10$ ,  $G_{2L} = 8$ ,  $G_{2W} = 8$ ,  $W_F = 2$ ,  $W_{F1} = 0.61$ ,  $W_{F2} = 0.5$ ,  $W_{F3} = 0.5$ ,  $G_p = 0.2$ ,  $G_{p1} = 0.3$ ,  $G_{p2} = 0.2$ ,  $S_L = 5$ ,  $r = 2$ ,  $d = 0.035$ : all dimensions are in millimetres]

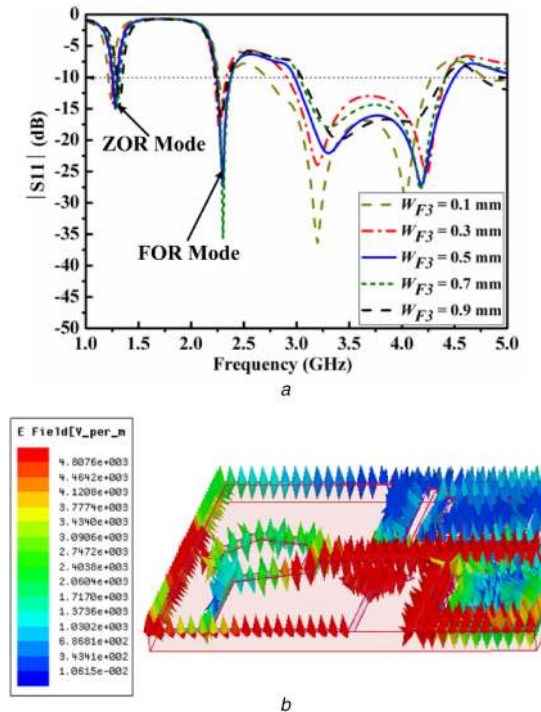


**Fig. 3** Input reflection coefficient  $E$ -field distribution of the proposed triple-band MTM antenna

(a) Input reflection coefficient of the proposed triple-band MTM antenna by varying ( $W_{F3}$ ) width of stripline,

(b) Simulated  $E$ -field distribution of the proposed triple-band MTM antenna at ZOR frequency

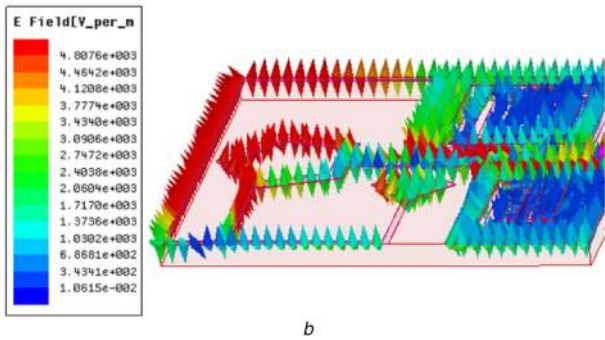
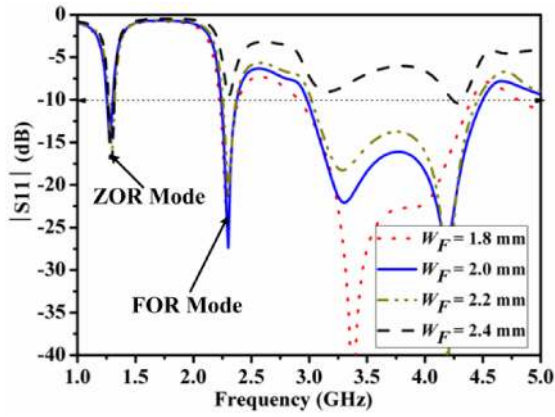


**Fig. 4** Input reflection coefficients of the proposed triple-band MTM antenna

- (a) Input reflection coefficient of the proposed triple-band MTM antenna by varying ( $W_F$ ) width of the series inductor,
- (b) Simulated  $E$ -field distribution of the proposed triple-band MTM antenna at FOR frequency

### 2.4 Effect of CCCRR

It can be observed in Fig. 5 that with an addition of the CCCRR, which is etched from the asymmetric ground plane, improves the impedance matching and gain of the MTM antenna. The CCCRRs on both sides of the asymmetric ground plane generate higher coupling capacitance and lower inductance values, which help in improving the gain at ZOR mode and better impedance matching at higher-order mode (2.98–4.5 GHz), as shown in Figs. 5b and a.

## 3 Antenna operation mechanism

To understand the operating principle of the proposed MTM antenna, four antenna prototypes (Antenna-1–Antenna-4) which are useful for understanding the evolution of the final structure (Antenna-5) are shown in Fig. 6. The input reflection coefficients and peak gains for Antenna-1–Antenna-5 are shown in Fig. 7.  $E$ -field distributions in the final proposed structure are shown in Fig. 8 for identifying the generation of the band and its effects on antenna performance.

Design starts with CPW fed having a hollow pentagonal radiator called as Antenna-1 as shown in Fig. 6a. It can be observed from Fig. 7 that the  $-10$  dB impedance bandwidth for Antenna-1 is very less.

So for the improvement of  $-10$  dB impedance bandwidth, the asymmetric ground plane has been created, called Antenna-2, as shown in Fig. 6b. This asymmetric ground plane increases the capacitive part of the proposed antenna which results in higher bandwidth but with less matching, shown in Fig. 7a.

For balancing the capacitive part of the proposed antenna, a thin strip inductive part is added to the asymmetric ground plane and terminated by the half-bowtie-shaped stub, called as Antenna-3, and shown in Fig. 6c. By adding the thin strip, proper matching with  $-10$  dB impedance bandwidth of 50% (3–5 GHz) can be observed in Fig. 7a.

Antenna-4 has been designed by adding another strip ( $S_{L2}$ ) to the Antenna-3 as shown in Fig. 6d. This strip is connected to the

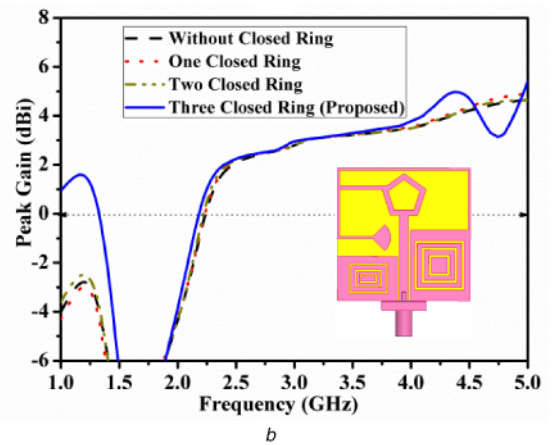
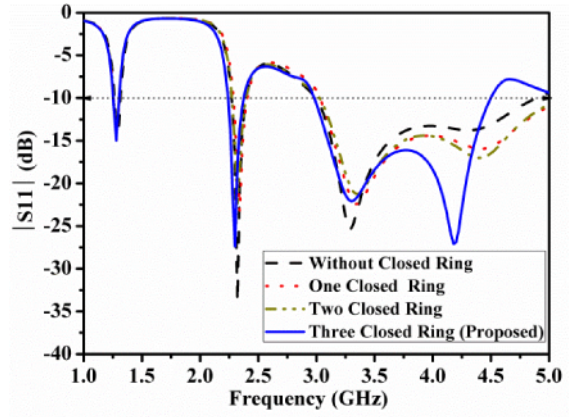


**Fig. 5** Effect of addition of CCCRR on the asymmetric ground plane  
(a) Input reflection coefficients,  
(b) Peak gain

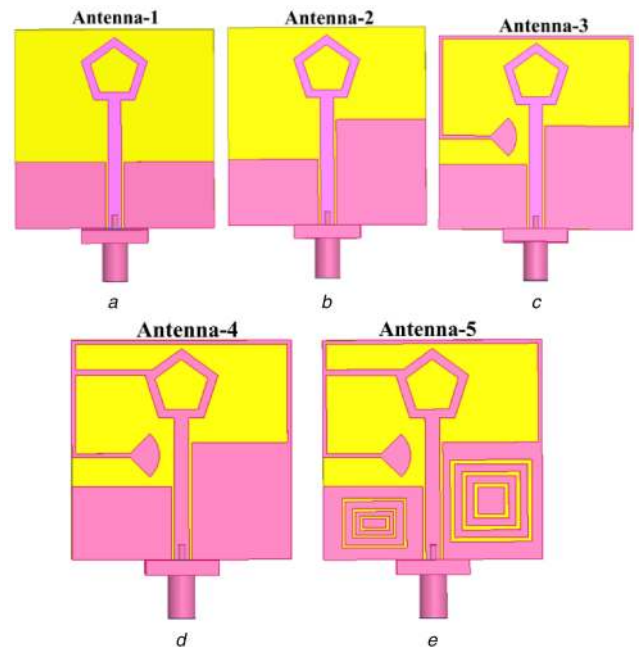


**Fig. 6** Evolution procedure of the proposed triple-band MTM antenna  
(a) Antenna-1,  
(b) Antenna-2,  
(c) Antenna-3,  
(d) Antenna-4,  
(e) Antenna-5 (proposed)

main radiator, i.e. between hollow pentagonal and the thin strip inductive part, which provides more paths for the current to flow. This results in the generation of two extra frequency bands on the lower side, as shown in Fig. 7a. It can be observed from Fig. 7b

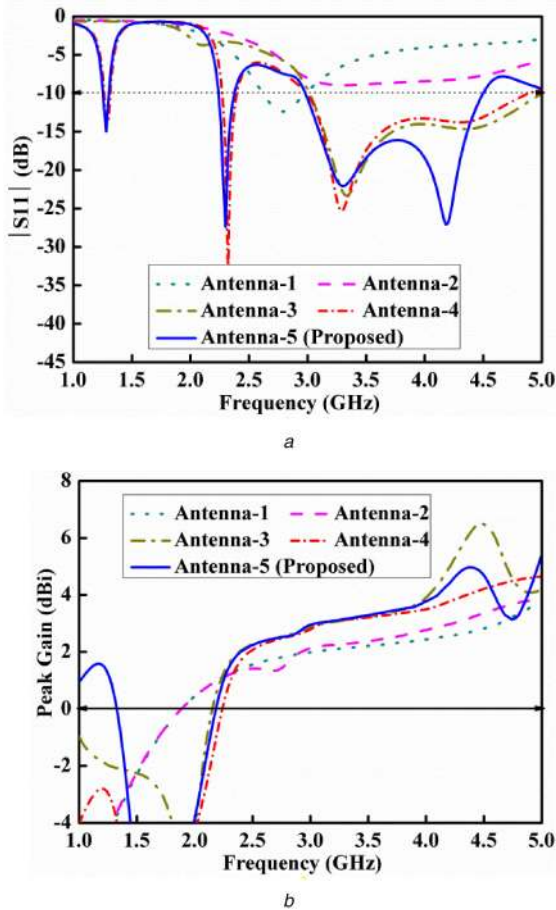


**Fig. 7** Results of evolution procedure of the proposed triple-band MTM antenna

- (a) Input reflection coefficients,  
(b) Peak gain

that the peak gain of the first band is negative while the other two bands are positive.

So, to increase the gain of the first band, CCCRRs on both sides of the ground plane have been added, called Antenna-5, as shown in Fig. 6e. By the addition of CCCRRs on both sides, the first band shows positive gain and improves matching of higher-order modes because it offers high value of capacitance and suppresses surface waves.

Explanation of the evolution of the final proposed structure is given in this section by plotting  $E$ -field distributions.

It can be recognised apparently that the first resonating frequency of 1.28 GHz is due to coupling between half-bowtie stub, a series inductor and left-hand side of the ground plane, as shown in Fig. 8a. The combination of all three elements is responsible for generating the first band of the proposed antenna. It can be observed from Fig. 8b that the second resonating frequency 2.3 GHz is due to the combined effects of a thin strip, hollow pentagonal and the coupling between the patch and both ground planes.

In case of third band generation, third resonating frequency 3.3 GHz is due to coupling between the patch and right-hand side ground plane (see Fig. 8c) while the fourth resonating frequency 4.2 GHz is due to the asymmetric ground and patch, as shown in Fig. 8d. This concludes that the third band is generated due to the combined effects of asymmetric ground plane and patch.

#### 4 Simulated and experimental results

To verify the simulated near- and far-field results done in high-frequency structure simulator software, the antenna prototype has been fabricated as shown in Fig. 9a. The measurements are carried out by using the Keysight Programmable Network Analyser (N5221A). Fig. 9b presents the experimental results of the input

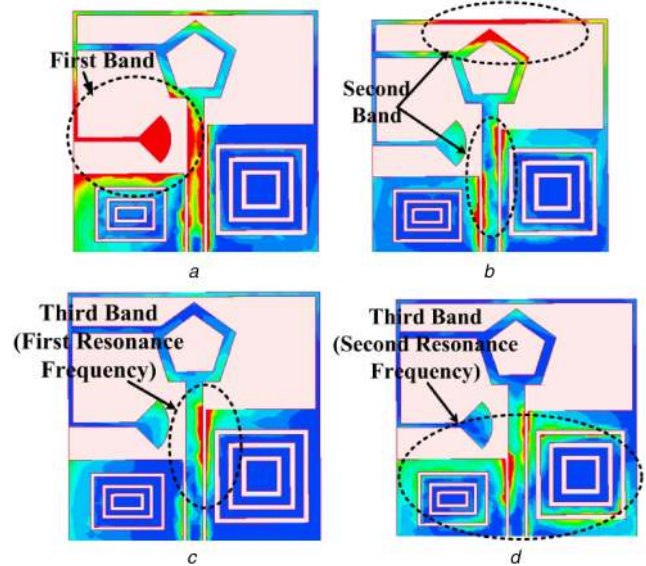


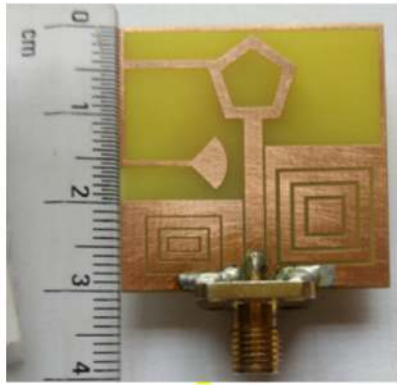
**Fig. 8**  $E$ -field distribution of the proposed triple-band MTM antenna

- (a) 1.28 GHz,  
(b) 2.3 GHz,  
(c) 3.3 GHz,  
(d) 4.2 GHz

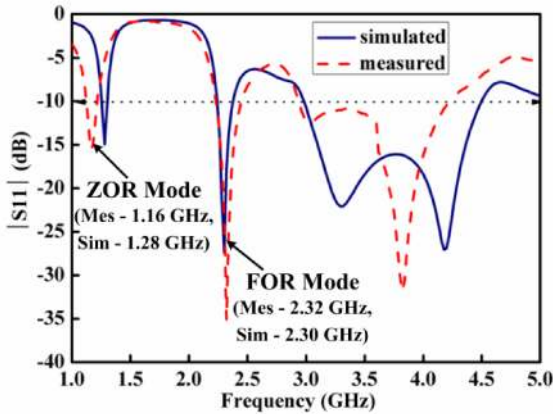
reflection coefficient ( $S_{11} < -10$  dB), which are in good agreement with the simulated results. The significant difference is observed subject to the fabrication tolerances and imperfection in soldering. The simulated triple-band MTM antenna offers  $-10$  dB input impedance bandwidth of 4.01% (1.25–1.30 GHz), 6.06% (2.24–2.38 GHz) and 40.64% (2.98–4.5 GHz), whereas the measured  $-10$  dB input impedance bandwidths of 8.54% (1.12–1.22 GHz), 10.25% (2.22–2.46 GHz) and 35.75% (2.94–4.22 GHz) are obtained at the three bands. The simulated resonant frequencies of ZOR and FOR are found to be 1.28 and 2.30 GHz, respectively, whereas the measured resonant frequencies are obtained at 1.16 and 2.32 GHz, respectively. Fig. 9c depicts the comparisons of input impedance extracted from the circuit model for both real and imaginary parts with the numerical simulations. It is clearly observed in Fig. 9c that the matching impedance of all the operating frequencies, i.e.  $f_{01} = 1.28$  GHz,  $f_{02} = 2.30$  GHz,  $f_{03} = 3.30$  GHz and  $f_{04} = 4.20$  GHz are found to be nearly  $50 \Omega$  from both the simulations and circuit model.

The normalised simulated and measured radiation patterns at ZOR and FOR modes are plotted in both the  $xz$ -plane ( $E$ -plane) and the  $yz$ -plane ( $H$ -plane) as shown in Fig. 10, whereas Fig. 11 shows the other higher-order modes. From both Figs. 10 and 11, it can be observed that the proposed triple-band MTM antenna provides an omnidirectional pattern in the  $E$ -plane and dipolar type pattern in the  $H$ -plane. The proposed triple-band MTM antenna offers simulated cross-polarisation level as below as  $-13.02$  dB in the  $E$ -plane and  $-14.53$  dB in the  $H$ -plane at ZOR frequency, whereas measured cross-polarisation level is as below as  $-12.47$  dB in the  $E$ -plane and  $-13.34$  dB in the  $H$ -plane in the direction of maximum radiation. In case of FOR mode and other higher-order modes, the measured co- and cross-polarisation radiation patterns in  $E$  and  $H$  planes are slightly different from the simulated one. It happened because of the asymmetrical antenna structure and measurement inaccuracy.

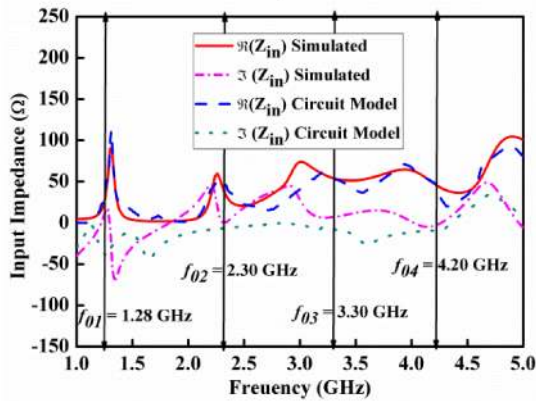
Fig. 12a depicts the simulated and measured gains in broadside direction and it can be observed that the designed MTM antenna shows the simulated gain of 0.97, 1.50 and 3.69 dBi in the first, second and third bands, respectively, whereas the measured gain shows 0.61, 0.96 and 2.74 dBi in the first, second and third bands, respectively. The simulated radiation efficiency of the proposed MTM antenna shows 71.81, 77.53 and 92.79% in the first, second and third bands, respectively, whereas the measured radiation efficiencies of first, second and third bands are 68.35, 66.96 and 90.68%, respectively, as shown in Fig. 12b. Table 1 compares the proposed triple-band MTM antenna with the reference antennas.



a



b



c

**Fig. 9** Fabricated antenna and results of input reflection coefficients of the proposed triple-band MTM antenna

(a) Simulated and measured reflection coefficients,

(b) Photograph,

(c) Input impedance extracted from the circuit model for both real and imaginary parts with the numerical simulations

Comparison table shows that the proposed MTM antenna is significantly smaller in the area, and also having high-impedance bandwidth with a better level of average gain and radiation efficiency as compared with the other reported published works.

## 5 Conclusion

A compact planar and asymmetric CPW-fed triple-band MTM inspired antenna using open-ended configuration has been designed, fabricated and tested. The antenna is designed based on ENG-TL, so that the bandwidth characteristics of the ZOR and FOR are analysed as per the ENG-TL theory. The proposed MTM antenna is based on the open-ended condition; therefore, the ZOR mode can be controlled by using shunt LC elements, whereas FOR mode depends on both series and shunt LC-LC parameters. Here, CCCRRs are specially used for increasing ZOR gain and also for

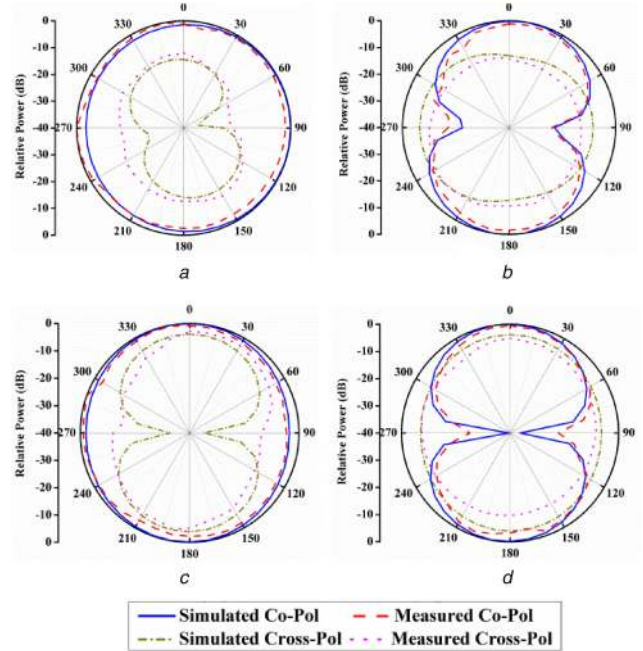


**Fig. 10** Normalised radiation patterns of the proposed triple-band MTM antenna

(a) E-plane, 1.28 GHz,

(b) H-plane, 1.28 GHz,

(c) E-plane, 2.30 GHz,

(d) H-plane, 2.30 GHz

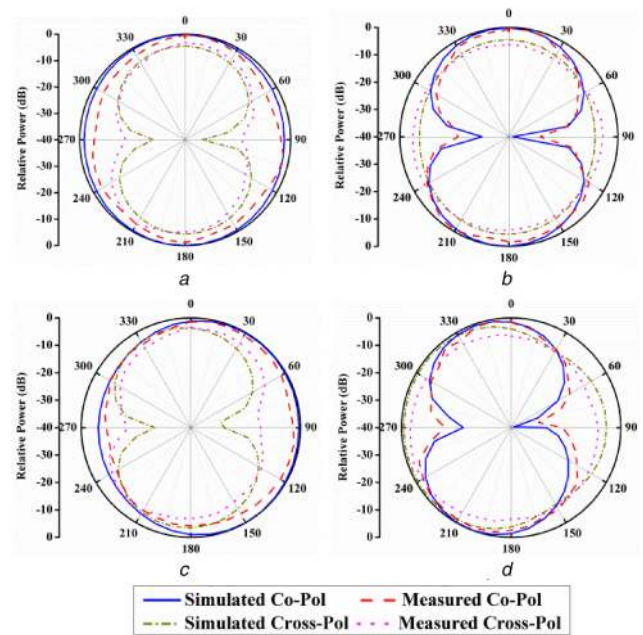


**Fig. 11** Normalised radiation patterns of the proposed triple-band MTM antenna

(a) E-plane, 3.30 GHz,

(b) H-plane, 3.30 GHz,

(c) E-plane, 4.20 GHz,

(d) H-plane, 4.20 GHz

improving the matching characteristics in higher-order modes. The designed antenna is miniaturised in size ( $0.11\lambda_0 \times 0.11\lambda_0 \times 0.006\lambda_0$ ) and offers measured triple-band fractional impedance bandwidths of 8.54, 10.25 and 35.75% for three bands. The proposed MTM antenna gives omnidirectional and dipolar type radiation patterns in the E-plane and the H-plane, respectively, in all the triple bands. The designed MTM antenna provides triple-band characteristics, high level of miniaturisation, higher peak gain and good radiation

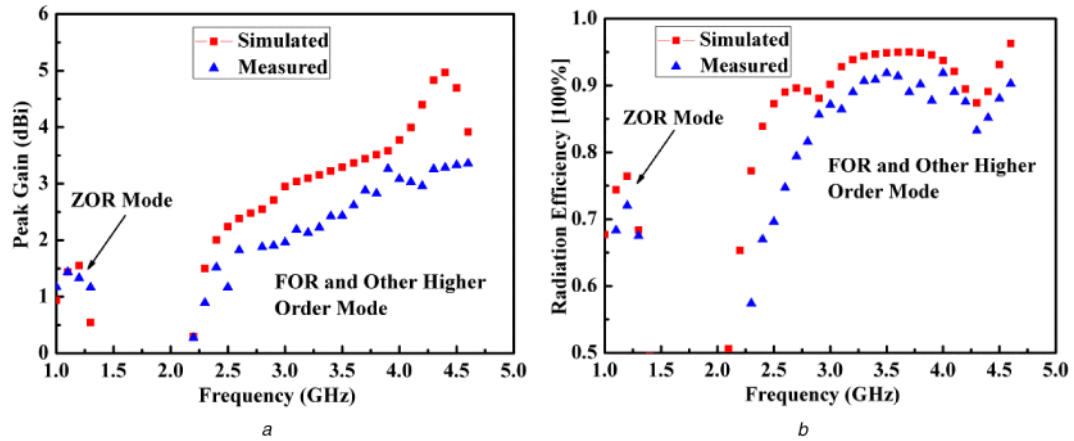


**Fig. 12** Simulated and measured far-field results (gain and radiation efficiencies) in the broadside direction of the proposed triple-band MTM antenna  
 (a) Peak gain,  
 (b) Radiation efficiency

**Table 1** Comparison of the proposed triple-band MTM antenna with reference antennas results

Overall size of antenna element	This work				[21]		[17]		
	$0.11\lambda_0 \times 0.11\lambda_0 \times 0.006\lambda_0$ ( $30 \times 30 \times 1.6 \text{ mm}^3$ )	$0.31\lambda_0 \times 0.28\lambda_0 \times 0.011\lambda_0$ ( $45 \times 40 \times 1.6 \text{ mm}^3$ )	$0.09\lambda_0 \times 0.077\lambda_0 \times 0.11\lambda_0$ ( $35 \times 38 \times 1 \text{ mm}^3$ )						
resonant frequency, GHz	1.16	2.32	3.58	2.08	4.31	5.50	1.81	3.1	5.81
impedance	8.54	10.25	35.75	5.76	0.46	2	3.31	49.03	2.06
bandwidth, %									
maximum gain, dBi	1.59	2.10	4.97	1.87	2.90	4.13	NA <sup>#</sup>	NA <sup>#</sup>	NA <sup>#</sup>
maximum radiation efficiency, %	73%	82%	95%	57.07	57.53	73.1	NA <sup>#</sup>	NA <sup>#</sup>	NA <sup>#</sup>

NA<sup>#</sup> = not available.

efficiency. The proposed MTM antenna is more suitable for modern wireless communication systems which work in L, S and C bands.

## 6 Acknowledgments

This research work is supported by the Science and Engineering Research Board (SERB), DST, India under Project no. EEQ/2016/000023. The authors also thank Mr. Dilip Kumar Choudhary (SRF), Mr. Mohammad Ameen, JRF (SERB Project) and Mr. Thummaluru Sreenath Reddy (JRF), IIT(ISM) Dhanbad for providing assistance to improve the technical content and literature of this paper.

## References

- [1] Ramo, S., Whinnery, J.R., Duzer, T.V.: *Fields and waves in communication electronics* (Wiley, New York, 1984, 2nd edn.)
- [2] Lai, A., Itoh, T., Caloz, C.: 'Composite right/left-handed transmission line metamaterials', *IEEE Microw. Mag.*, 2004, 5, pp. 34–50
- [3] Lai, A., Leong, K.M.K.H., Itoh, T.: 'Infinite wavelength resonant antennas with monopolar radiation pattern based on periodic structures', *IEEE Trans. Antennas Propag.*, 2007, 55, pp. 868–876
- [4] Ziolkowski, R.W., Erentok, A.: 'Metamaterial-based efficient electrically small antennas', *IEEE Trans. Antennas Propag.*, 2006, 54, pp. 2113–2130
- [5] Mishra, N., Chaudhary, R.K.: 'A miniaturized ZOR antenna with enhanced bandwidth for WiMAX applications', *Microw. Opt. Technol. Lett.*, 2016, 58, pp. 71–75
- [6] Sharma, S.K., Chaudhary, R.K.: 'A compact zeroth-order resonating wideband antenna with dual-band characteristics', *IEEE Antennas Wirel. Propag. Lett.*, 2015, 14, pp. 1670–1672
- [7] Cai, T., Wang, G.-M., Zhang, X.-F., et al.: 'Compact microstrip antenna with enhanced bandwidth by loading magneto-electro-dielectric planar waveguided metamaterials', *IEEE Trans. Antennas Propag.*, 2015, 63, pp. 2306–2311
- [8] Cai, T., Wang, G.-M., Zhang, X.-F., et al.: 'Low-profile compact circularly-polarized antenna based on fractal metasurface and fractal resonator', *IEEE Antennas Wirel. Propag. Lett.*, 2015, 14, pp. 1072–1076
- [9] Sanada, A., Caloz, C., Itoh, T.: 'Novel zeroth-order resonance in composite right/left-handed transmission line resonators', *Proc. Asia-Pac. Microw. Conf.*, 2003, 3, pp. 1588–1591
- [10] Eleftheriades, G.V., Iyer, A.K., Kremer, P.C.: 'Planar negative refractive index media using periodically LC loaded transmission lines', *IEEE Trans. Microw. Theory Tech.*, 2002, 50, pp. 2702–2712
- [11] Park, J.H., Ryu, Y.H., Lee, J.G., et al.: 'Epsilon negative zeroth order resonating antenna', *IEEE Trans. Antennas Propag.*, 2007, 55, pp. 3710–3712
- [12] Sharma, S.K., Gupta, A., Chaudhary, R.K.: 'Epsilon negative CPW-fed zeroth-order resonating antenna with backed ground plane for extended bandwidth and miniaturization', *IEEE Trans. Antennas Propag.*, 2015, 63, pp. 5197–5203
- [13] Kukreja, J., Choudhary, D.K., Chaudhary, R.K.: 'CPW fed miniaturized dualband short-ended metamaterial antenna using modified split-ring resonator for wireless application', *Int. J. RF Microw. Comput. Aided Eng.*, 2017, 27, (8), pp. 1–7, Available at e21123, doi: 10.1002/mmce.21123
- [14] Niu, B.-J., Feng, Q.-Y.: 'Bandwidth enhancement of asymmetric coplanar waveguide (ACPW)-fed antenna based on composite right/left handed transmission line', *IEEE Antennas Wirel. Propag. Lett.*, 2013, 12, pp. 563–566
- [15] Li, L., Jia, Z., Huo, F., et al.: 'A novel compact multiband antenna employing dual-band CRLH-TL for smart mobile phone application', *IEEE Antennas Wirel. Propag. Lett.*, 2013, 12, pp. 1688–1691
- [16] Amani, N., Kamyab, M., Jafarholi, A., et al.: 'Compact tri-band metamaterial-inspired antenna based on CRLH resonant structures', *Electron. Lett.*, 2014, 50, pp. 847–848
- [17] Zhu, C., Li, T., Li, K., et al.: 'Electrically small metamaterial-inspired tri-band antenna with meta-mode', *IEEE Antennas Wirel. Propag. Lett.*, 2015, 14, pp. 1738–1741
- [18] Caloz, C., Itoh, T.: *Electromagnetic metamaterials: transmission line approach and microwave applications* (Wiley, Hoboken, NJ, USA, 2005)
- [19] Niu, B.-J., Feng, Q.-Y.: 'Bandwidth enhancement of CPW-fed antenna based on epsilon negative zeroth and first-order resonators', *IEEE Antennas Wirel. Propag. Lett.*, 2013, 12, pp. 1125–1128
- [20] Chiu, S.-C., Lai, C.-P., Chen, S.-Y.: 'Compact CRLH CPW antennas using novel termination circuits for dual-band operation at zeroth-order series and shunt resonances', *IEEE Trans. Antennas Propag.*, 2013, 61, pp. 1071–1080
- [21] Gupta, A., Chaudhary, R.K.: 'A compact planar metamaterial triple-band antenna with complementary closed-ring resonator', *Wirel. Pers. Commun.*, 2016, 88, pp. 203–210